nature communications

Article

https://doi.org/10.1038/s41467-025-68060-1

Multi-omics analysis identifies a microbiota–bile acid–TLR signaling axis driving bladder injury in interstitial cystitis

Received: 13 June 2023

Accepted: 16 December 2025

Published online: 29 December 2025

Check for updates

Liao Peng[1,5], Jia-wei Chen[1,5], Yuan-zhuo Chen[1,5], Xing-peng Di[1,5], Le-de Lin[1,5], Bo-ya Li[1,2,5], Chi Zhang[1,5], Wei Wang[1], Xiao-shuai Gao[1], Yu-cheng Ma[1], Si-hong Shen[1], Hai-rui Li[1], Xiao-fang Xu[3], Xiao Zeng[1], Hong Shen[1], Qun Sun[3] ✉, Tao Jin[1,4] ✉ & De-yi Luo[1,4] ✉

Hunner-type interstitial cystitis/bladder pain syndrome (HIC) is a debilitating condition defined by bladder pain and urinary urgency, yet its upstream drivers remain poorly understood. To identify upstream mechanisms that exacerbate urothelial injury, here we apply an integrative multi-omics framework combining metagenomic sequencing, targeted metabolomics of urine and serum, and single-cell RNA sequencing. This approach reveals a microbial signature enriched in *Enterococcus avium* and a marked alteration in bile acid metabolism, including increased taurochenodeoxycholic acid (TCDCA). Single-cell analysis indicates that these changes converge on Toll-like receptor 3 (TLR3) activation in urothelial cells. Further validations show that a microbiota–bile acid–TLR3 axis disrupts epithelial barrier integrity and triggers inflammatory responses in experimental models. Transplantation and metabolite administration confirm the causal role of *E. avium* and TCDCA, while TLR3 inhibition ameliorates injury. These findings uncover an upstream pathway linking gut-derived metabolites to bladder pathology and suggest opportunities for biomarker development and targeted therapies for HIC.

Interstitial cystitis/bladder pain syndrome (IC/BPS) currently represents one of the most challenging diseases, with an approximate prevalence of 45 cases per 100,000 individuals[1]. The elusive pathophysiological mechanism has impeded significant advancements in the treatment of IC/BPS[1,2], in stark contrast to the progress made over the past 30 years. Moreover, the recurrence rate after stepwise treatments is ~40–50%, leading some patients to undergo cystectomy for pain relief[2,3]. In line with the reported mechanisms, our previous studies[4,5] found the disruption of the epithelial barrier and the abnormal activation of the immune response emerge as pivotal pathophysiological processes in IC/BPS patients. Nonetheless, the underlying cause of these pathological changes within the bladder remains uncertain.

IC/BPS is increasingly recognized as a systemic disease involving multiple organ systems, although its clinical symptoms are predominantly localized to the bladder. To identify upstream drivers of bladder injury and potential biomarkers of IC/BPS, previous studies have examined alterations in the gut and urinary microbiota[6,7], bladder transcriptomes[4], and both blood and urine metabolomes[7–9]. Among these foundational studies, only one study[6] analyzed the gut microbiota composition using 16S ribosomal RNA (rRNA) gene sequencing, reporting elevated levels of *Eubacterium sinensis*, *Collinsella*

[1]Department of Urology, Institute of Urology (Laboratory of Reconstructive Urology), West China Hospital, Sichuan University, Chengdu, Sichuan, China. [2]Department of Pediatric Surgery, Sichuan Academy of Medical Sciences Sichuan Provincial People's Hospital, Chengdu, China. [3]Key Laboratory of Bio-resources and Eco-environment of the Ministry of the Education, College of Life Sciences, Sichuan University, Chengdu, Sichuan, China. [4]Pelvic Floor Diseases Center, West China Tianfu Hospital, Sichuan University, Chengdu, Sichuan, China. [5]These authors contributed equally: Liao Peng, Jia-wei Chen, Yuan-zhuo Chen, Xing-peng Di, Le-de Lin, Bo-ya Li, Chi Zhang. ✉e-mail: qunsun@scu.edu.cn; jintao97@scu.edu.cn; luodeyi1985@163.com

aerofaciens, *Faecalibacterium prausnitzii*, *Oscillibacter splanchnicus*, and *Lactobacillus longoviformis* in IC/BPS patients. However, due to the limited taxonomic resolution of 16S rRNA sequencing, the specific microbial species contributing to urothelial injury remain unclear. Similarly, only one study[9] examined the blood metabolome, identifying anandamide and linoleic acid-associated lipids as potential discriminators between IC/BPS and overactive bladder. In contrast, most existing research has focused on urinary microbiota, metabolites, and cytokines. Several recent reviews[10–13] summarized potential urinary biomarkers based on the previously published studies, including bacterial genera such as *Ralstonia* and *Lactobacillus*, metabolites such as tetradecylamine and glyceraldehyde, and cytokines such as *TNF-α*, *IL-6*, and *NGF*. However, findings across studies have been inconsistent, and further validation of these candidates remains scarce. More importantly, no studies integrated changes across the gut–blood–urine–bladder axis in IC/BPS to identify systemic factors that contribute to urothelial injury. Therefore, these gaps highlight the pressing need for integrative multi-omics approaches that can comprehensively characterize disease-associated changes and enable mechanistic validation through both in vitro and in vivo experiments.

Urothelial injury is a hallmark feature of IC/BPS, both in patients with and without Hunner lesions (HLs)[2]. Patients with HLs exhibit more severe lower urinary tract symptoms (LUTS), heightened inflammatory responses, and a greater degree of urothelial denudation compared to those without HLs[14]. Hunner-type IC/BPS (HIC) is considered a more severe phenotype, highlighting the critical importance of elucidating the mechanisms underlying urothelial injury in this disorder. Such investigations hold great potential for advancing the development of targeted therapies and preventive strategies across all subtypes of IC/BPS.

In this work, we firstly integrate metagenomic sequencing, targeted metabolomic profiling of urine and blood, and single-cell RNA sequencing to elucidate the mechanisms underlying urothelial injury in HIC. This multi-omics approach overcomes key limitations of previous studies, including the low resolution of 16S rRNA sequencing, the lack of metabolite specificity, and the uncertainty regarding the injury-related cell types. Our analysis identifies a potential mechanistic axis, *E. avium*-TCDCA-TLR3, that may drive the development and progression of HIC. This axis is further validated through both in vitro and in vivo experiments. Collectively, these findings advance our understanding of HIC pathogenesis and provide potential biomarkers for diagnosis, as well as therapeutic targets for personalized treatment strategies.

Results

Altered microbial profile and function in patients with HIC

As shown in Supplementary Table 1, 50 female patients with HIC and 54 female controls were enrolled according to predefined inclusion and exclusion criteria (Supplementary Table 2). No significant differences were found between the groups in age, BMI, or menopausal status. Compared to controls, HIC patients exhibited significantly higher voiding frequency, nocturia, and increased ICSI, ICPI, and VAS scores.

As for microbial composition analysis, Core, Pan, and Coverage index analyses confirmed sufficient sample size for microbial profiling (Supplementary Fig. 1A–C). In terms of α-diversity, the Simpson, Shannon, Chao, and ACE indices showed no significant differences between the two groups, indicating comparable microbial richness and diversity (Supplementary Fig. 1D). However, β-diversity analysis showed distinct microbial compositions between the two groups ($p = 0.001$) (Fig. 1A). A total of 46 and 64 unique OTUs were identified in the HIC and control groups, respectively (Supplementary Fig. 1E). At the phylum level, Firmicutes was the most abundant (68.88%) (Supplementary Fig. 1F). At the genus level, LEfSe analysis revealed higher abundances of *UCG-002* and *Hungatella*, and decreased levels of *Megamonas* and *Roseburia* in HIC patients (Fig. 1B and Supplementary Fig. 1G).

Notably, few studies have investigated gut microbiota in IC/BPS. To date, only one human study using 16S rDNA sequencing reported reduced levels of *E. sinensis*, *C. aerofaciens*, *F. prausnitzii*, *O. splanchnicus*, and *L. longoviformis* in IC/BPS patients[6]-partially consistent with our findings (Supplementary Fig. 1G).

Given that 16S rRNA sequencing is limited to genus-level resolution, we performed the first metagenomic sequencing analysis of fecal samples in HIC to gain a more comprehensive understanding of microbial alterations. At the species level, α-diversity showed no differences between the two groups (Fig. 1C), but distinct compositional changes were identified (Fig. 1D). *Enterococcus avium, Megasphaera micronuciformis*, and *Fusobacterium nucleatum* were enriched in the HIC group, while *Anaerostipes hadrus* and *Collinsella aerofaciens* dominated in controls (Fig. 1E). Notably, the functions of differentially abundant species in HIC were primarily linked to bile acid (BA) metabolism (Fig. 1F, G), suggesting that specific microbial alterations—particularly *E. avium*, *M. micronuciformis*, and *F. nucleatum*—may contribute to dysregulated BA metabolism. Despite the diagnostic complexity of HIC, a specificity of 0.881 (CI: 0.785–0.978) was achieved using the top three differential species (Fig. 1H).

In conclusion, the first metagenomic analysis of HIC gut microbiota reveals possible BA metabolism-related microbial shifts, highlighting *E. avium*, *M. micronuciformis*, and *F. nucleatum* as potential diagnostic biomarkers.

Blood and urine metabolomic analysis reveals BA-related metabolic alterations

Although metagenomic analysis indicated that differential microbial species were associated with BA metabolism, it remained unclear whether other metabolic pathways contribute to HIC pathogenesis. To address this, we performed metabolomic profiling of blood and urine samples from HIC patients and healthy controls.

After standard quality control, PCA (Supplementary Fig. 1H, I) and OPLS-DA analyses were performed to visualize metabolic distributions and identify differential metabolites between groups. The OPLS-DA results showed a clear separation between HIC patients and controls (Fig. 2A, B). In total, 77 differential metabolites were identified in blood, with the majority classified as lipids and lipid-like molecules (36.65%) (Fig. 2C). In urine, 168 differential metabolites were detected, primarily comprising organic acids and derivatives (26.95%) (Fig. 2D). Pathway enrichment analysis revealed significant metabolic alterations in HIC patients, with notable enrichment in bile secretion, protein digestion and absorption, and primary bile acid biosynthesis pathways in serum (Fig. 2E). Strikingly, bile acid metabolism—including bile secretion, secondary bile acid biosynthesis, and cholesterol metabolism—was also the most enriched pathway in urine samples (Fig. 2F).

Although BA metabolism has not been rarely reported in IC/BPS, a prior study identified the bile acid receptor TGR5 as a key mediator of bladder afferent hypersensitivity[15], supporting a potential mechanistic link. To further pinpoint specific altered metabolites, we quantized BA-associated metabolites in both blood and urine. Notably, taurochenodeoxycholic acid (TCDCA) and tauroursodeoxycholic acid (TUDCA) were concurrently elevated in both compartments of HIC patients (Fig. 2G, H).

In summary, metabolomic profiling confirmed a systemic upregulation of BA metabolism in HIC, consistent with the functional analysis of differential microbial species (Fig. 1H), and highlighted TCDCA and TUDCA as potential key metabolites driving disease development and progression.

Single-cell RNA sequencing suggests involvement of TLR signaling in urothelial injury in HIC

Given the observed alterations in microbial species (Fig. 1E) and the elevated levels of urinary TCDCA and TUDCA (Fig. 2G, H), we hypothesized that these factors may contribute to urothelial injury.

https://doi.org/10.1038/s41467-025-68060-1

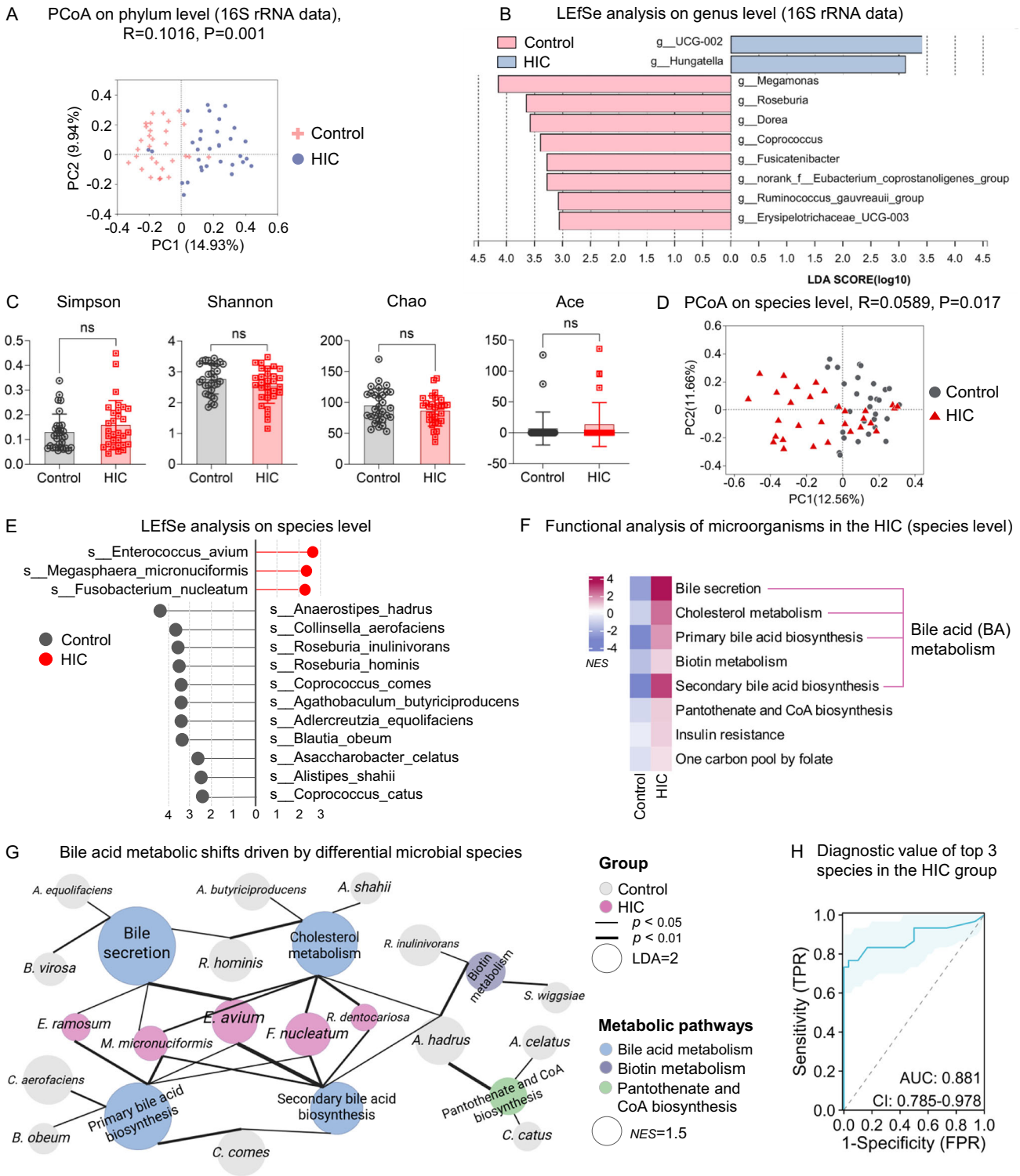

Fig. 1 | Microbial composition and functional alterations in patients with Hunner-type interstitial cystitis/bladder pain syndrome (HIC). A β-diversity analysis based on 16S rRNA sequencing, assessed by principal coordinates analysis (PCoA) using Bray–Curtis distances ($n = 30$ control vs. 32 HIC; two-sided PERMANOVA with 1000 permutations; multiple testing not applicable). **B** Differential bacterial genera identified by LEfSe analysis (LDA score ≥ 3 and $p < 0.05$; $n = 30$ control vs. 32 HIC; multiple testing not applicable). **C** Comparison of α-diversity based on metagenomic sequencing ($n = 30$ vs. 30; data show median (IQR); two-sided Mann–Whitney U test; ns not significant; multiple testing not applicable). **D** Comparison of β-diversity based on metagenomic sequencing. **E** Differential species identified by LEfSe. **F** Functional enrichment analysis of differential species in the HIC group. **G** Correlation network based on differential species and metabolic pathways. Pairwise associations were calculated using two-sided Spearman correlation. Significant correlations were defined as $p < 0.05$ and are represented as edges in the network. No multiple-testing correction was applied, as these analyses were exploratory. **H** Diagnostic performance (AUC) of the top three differential species for HIC classification. Source data are provided as a Source Data file.

https://doi.org/10.1038/s41467-025-68060-1

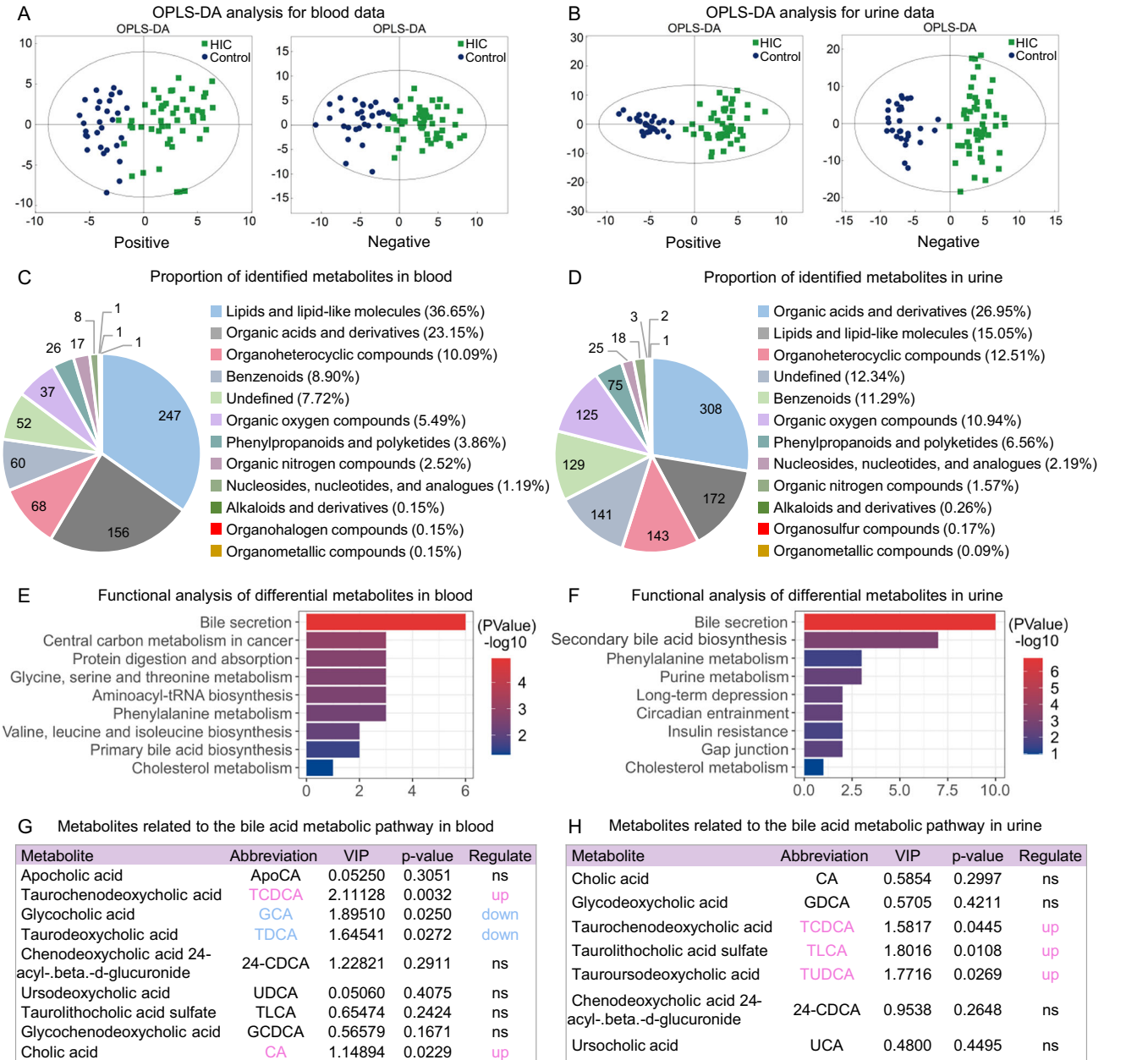

G Metabolites related to the bile acid metabolic pathway in blood

Metabolite	Abbreviation	VIP	p-value	Regulate
Apocholic acid	ApoCA	0.05250	0.3051	ns
Taurochenodeoxycholic acid	TCDCA	2.11128	0.0032	up
Glycocholic acid	GCA	1.89510	0.0250	down
Taurodeoxycholic acid	TDCA	1.64541	0.0272	down
Chenodeoxycholic acid 24-acyl-.beta.-d-glucuronide	24-CDCA	1.22821	0.2911	ns
Ursodeoxycholic acid	UDCA	0.05060	0.4075	ns
Taurolithocholic acid sulfate	TLCA	0.65474	0.2424	ns
Glycochenodeoxycholic acid	GCDCA	0.56579	0.1671	ns
Cholic acid	CA	1.14894	0.0229	up
Tauroursodeoxycholic acid	TUDCA	1.65523	0.0043	up

H Metabolites related to the bile acid metabolic pathway in urine

Metabolite	Abbreviation	VIP	p-value	Regulate
Cholic acid	CA	0.5854	0.2997	ns
Glycodeoxycholic acid	GDCA	0.5705	0.4211	ns
Taurochenodeoxycholic acid	TCDCA	1.5817	0.0445	up
Taurolithocholic acid sulfate	TLCA	1.8016	0.0108	up
Tauroursodeoxycholic acid	TUDCA	1.7716	0.0269	up
Chenodeoxycholic acid 24-acyl-.beta.-d-glucuronide	24-CDCA	0.9538	0.2648	ns
Ursocholic acid	UCA	0.4800	0.4495	ns
Deoxycholic acid	DCA	0.6071	0.6185	ns

Fig. 2 | Blood and urine metabolomic analysis reveals bile acids (BA)-related metabolic alterations. Visualization of metabolite distribution in blood (**A**) and urine (**B**) using orthogonal partial least-squares discriminant analysis (OPLS-DA; exploratory analysis; multiple testing not applicable). Categorization of differential metabolites in blood (**C**) and urine (**D**). Exploration of differential metabolic pathways in blood (**E**) and urine (**F**; two-sided hypergeometric test with FDR correction (Benjamini–Hochberg method); pathways with adjusted $p < 0.05$ are selected). BA-related metabolites in blood (**G**) and urine (**H**) ($n = 30$ control vs. 50 HIC; metabolites with VIP ≥ 1 from OPLS-DA and $p < 0.05$ from two-sided Mann–Whitney *U* test; exploratory analysis; *p*-values not adjusted). Source data are provided as a Source Data file.

Urothelial damage is a hallmark pathology in IC/BPS, despite cases with or without Hunner lesions[16]. Disruption of the urothelial barrier permits the translocation of toxic substances into the basal layer, lamina propria, and muscularis, contributing to the hallmark symptoms of IC/BPS, including urinary frequency, urgency, and pelvic pain[17]. To confirm the previous injury profile and identify new signaling pathways involved, we analyzed bulk RNA sequencing data from public databases and performed single-cell RNA sequencing on our own samples.

Bulk RNA sequencing revealed that differentially expressed genes (DEGs) (Supplementary Table 3) in the HIC bladder were significantly enriched in pathways related to barrier function, infection, BA metabolism, immune response, and inflammation (Fig. 3A–C). Further analysis highlighted inflammation- and barrier-related pathways, including Toll-like receptor (TLR) signaling, NOD-like receptor signaling, tight junctions, and focal adhesion (Fig. 3C). These findings align with our previous studies[4,5], and others[16,17], emphasizing the critical role of urothelial injury in HIC pathology.

To further refine the analysis, we examined DEGs (Supplementary Table 4) in urothelial cells (UCs) from single-cell RNA sequencing data (Fig. 3D). The cellular landscape of HIC bladder was established as our previous study[5]. Upregulated DEGs in UCs were associated with enhanced immune response, altered BA metabolism, increased apoptosis, and activation of inflammatory signaling, with TLR signaling emerging as the most significantly enriched pathway (Fig. 3E, F). Downregulated

https://doi.org/10.1038/s41467-025-68060-1

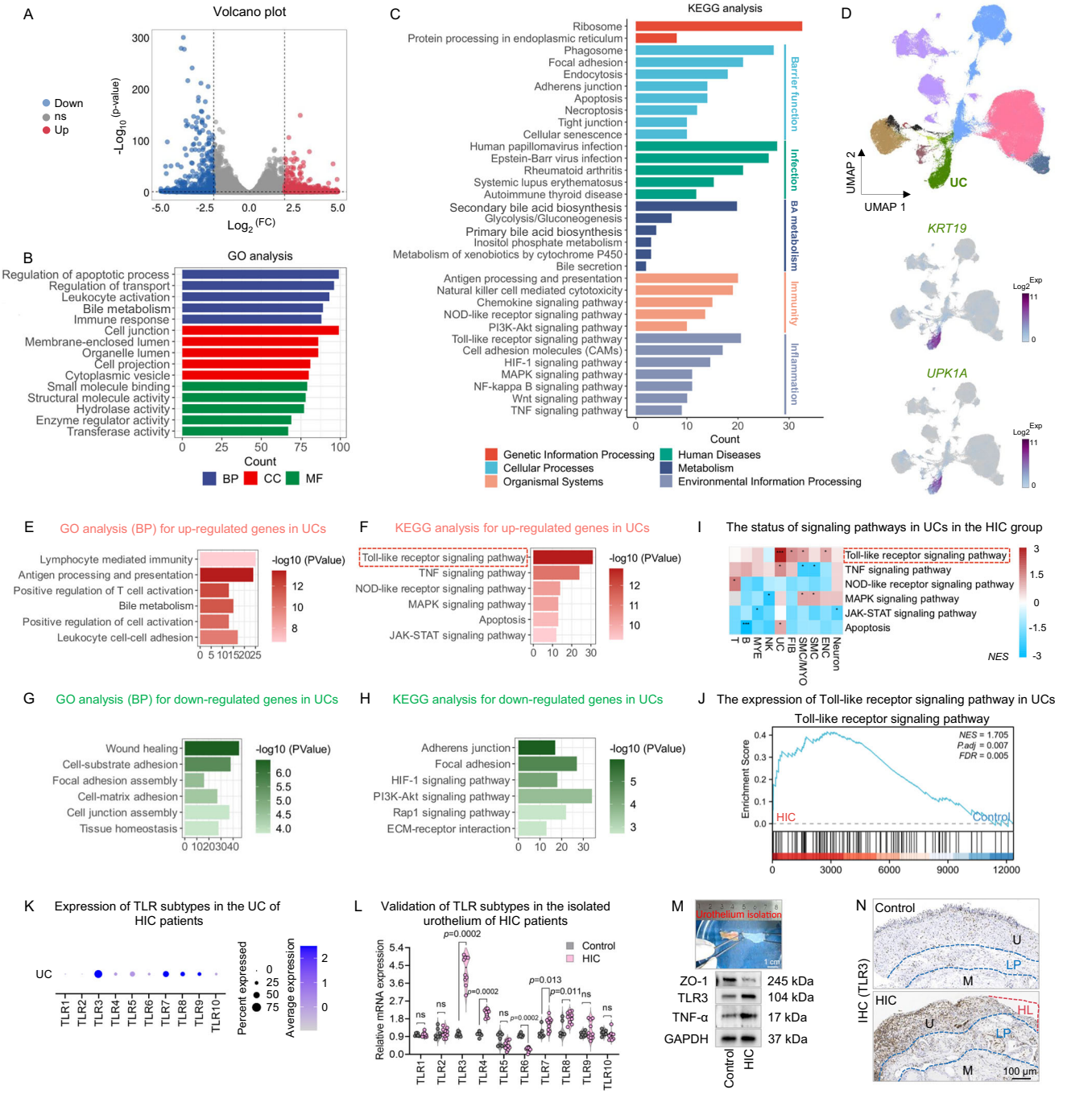

Fig. 3 | Single-cell RNA sequencing identifies TLR signaling as a key mediator of urothelial injury in HIC. A Differentially expressed genes (DEGs) in full-thickness bladder tissues from HIC patients and controls identified via RNA sequencing ($|\log_2 FC| \geq 2$; adjusted $p < 0.05$, two-sided Wald test using DESeq2). Gene Ontology (GO) (**B**) and KEGG (**C**) enrichment analyses of DEGs (two-sided hypergeometric test with FDR correction). **D** UMAP visualization of single-cell transcriptomic landscape of urothelium, with urothelial cells (UCs) identified by *KRT19* and *UPK1A* expression. GO (**E**) and KEGG (**F**) analyses of upregulated DEGs in UCs (two-sided hypergeometric test with FDR correction). GO (**G**) and KEGG (**H**) analyses of downregulated DEGs in UCs (two-sided hypergeometric test with FDR correction). **I**, **J** Gene Set Enrichment Analysis (GSEA) of altered pathways in UCs (two-sided permutation test with 1000 permutations, with multiple testing corrected using the FDR). The exact *p* value for TLR signaling of UCs in panel **I** is 0.0009. **K** Expression of Toll-like receptor (TLR) subtypes in UCs from HIC bladders. mRNA (**L**) and protein (**M**) expression levels of TLR3 in isolated urothelium from control and HIC patients ($n = 7$ control vs. 10 HIC; data show median (IQR); two-sided Mann–Whitney U test; ns not significant; Bar for panel M: 1 cm). **N** Immunostaining showing the distribution of TLR3 protein in the urothelium of patients with HIC ($n = 7$ control vs. 10 HIC; one section and field per patient; Bar: 100 μm). IHC immunohistochemistry, HL Hunner lesions, U urothelium, LP lamina propria (blue line), M muscularis. Source data are provided as a Source Data file.

DEGs were linked to impaired wound healing and disrupted tight junctions (Fig. 3G, H). Gene Set Enrichment Analysis (GSEA) further confirmed marked upregulation of TLR signaling in UCs from HIC bladders (Fig. 3I, J), suggesting its central role in mediating urothelial injury.

We then profiled TLR subtype expression in UCs from HIC bladders, identifying TLR3 as the most prominently upregulated receptor (Fig. 3K). This finding was further validated by assays performed on isolated bladder urothelium from HIC patients (using established

tissue isolation protocols[18]), which confirmed TLR3 overexpression (Fig. 3L–N and Supplementary Fig. 2A, B).

In summary, both bulk and single-cell transcriptomic analyses revealed disrupted barrier function, particularly tight junction impairment, and heightened inflammation in the HIC urothelium, with TLR signaling, especially TLR3, identified as a potential key driver of urothelial injury.

The crosstalk across altered gut microbiota, BA metabolic pathways, and bladder injury pathways

Multi-omics analyses suggested a potential link among altered microbial composition, dysregulated BA metabolism, and urothelial injury (characterized by tight junction impairment and TLR3 activation) in HIC. These alterations may collectively contribute to the development of lower urinary tract symptoms (LUTS) in affected patients. To further explore the interconnections and underlying crosstalk among these factors, a correlation network based on the matched participants was constructed. The results demonstrated that dominant bacteria in the HIC (*E. avium*, *M. micronuciformis*, and *F. nucleatum*) were positively correlated with elevated levels of TCDCA and TUDCA in both blood and urine (Fig. 4A, B). Given that urinary metabolites directly contact the urothelium and may exert damaging or protective effects, we specifically analyzed the associations of urinary TCDCA, TUDCA, and TLCA with TLR3 activation and tight junction integrity. TCDCA showed a positive correlation with TLR3 activation and a negative correlation with tight junction expression. In contrast, TUDCA exhibited the opposite pattern, suggesting a protective role (Fig. 4C, D). Consistently, the abundance of *E. avium* and *M. micronuciformis* in the HIC group was also positively associated with TLR3 signaling activation and tight junction disruption (Fig. 4E, F). Importantly, urinary TCDCA levels and *E. avium* abundance showed the strongest positive correlations with HIC symptom scores, including ICPI, ICSI, VAS, and 24-hour voiding frequency (Fig. 4G).

Among the altered bile acid metabolites, TCDCA is known to exert cytotoxic effects, as it induces mitochondrial permeability transition and Caspase-11–mediated pyroptosis in hepatocytes[19]. In contrast, TUDCA is a well-established inhibitor of endoplasmic reticulum stress, contributing to inflammatory homeostasis and metabolic regulation[20]. *E. avium* is frequently associated with polymicrobial infections, such as splenic abscesses[21], cholecystitis[22], and bacteremia[23], and is linked to a considerable crude mortality rate. Notably, *E. avium* can be isolated from bile fluid[22], further supporting a potential link between this species and BA metabolic dysfunction.

Correlation network analysis indicates that gut microbes, particularly *E. avium*, in HIC patients may contribute to systemic alterations in BA metabolism, marked by elevated levels of TCDCA and TUDCA. Among these metabolites, urinary TCDCA was specifically associated with urothelial injury, characterized by TLR3 signaling activation and barrier disruption. These findings suggest that the *E. avium*–TCDCA–TLR3 axis may constitute a key pathway underlying the development and progression of HIC.

Based on multi-omics findings, we proposed a mechanistic axis possibly mediating bladder injury in HIC and subsequently will validate this hypothesis through fecal microbiota transplantation (FMT), targeted bacterial colonization, and complementary in vivo and in vitro experiments.

HIC microbiota potentially modulates host metabolism and bladder response

To validate the potential crosstalk among gut microbiota, metabolism, and bladder injury, FMT was performed in antibiotic-treated mice (Abx-mice) using fecal samples from healthy controls and HIC patients (Fig. 5A). Bladder weights showed no significant differences across groups; however, the bladder-to-body weight ratio was higher in mice receiving fecal microbiota from HIC patients (Fig. 5B). Autoimmune cystitis (AC) mice exhibited a higher urination frequency, which slightly improved after receiving control FMT, whereas control mice receiving HIC-derived microbiota also showed increased urination frequency (Fig. 5C and Supplementary Fig. 2C). Pain behavior was similarly exacerbated in both AC and control mice following HIC FMT (Fig. 5D). Histological analysis revealed the marked abnormalities in the bladders of AC mice, including urothelial thinning, detachment, exposure, and thickening of the lamina propria. Immunohistochemistry (IHC) demonstrated the reduced ZO-1 expression and increased TNF-α and TLR3 levels, indicating the barrier disruption and enhanced inflammation in both AC and control mice after HIC FMT. In contrast, control FMT alleviated these pathological changes (Fig. 5E and Supplementary Fig. 2D). More importantly, urinary TCDCA and TUDCA levels were elevated in both AC and control mice after receiving HIC-derived microbiota (Fig. 5F).

These findings confirmed that FMT from HIC patients increased the urinary levels of TCDCA and TUDCA and exacerbated bladder injury in Abx-mice, supporting the potential microbiota-mediated link between altered bile acid metabolism and increased bladder susceptibility.

E. avium transplantation induces urothelial injury through TCDCA upregulation

Although we confirmed that FMT from Hunner-type IC/BPS patients increased urinary TCDCA and TUDCA levels and exacerbated bladder injury in Abx-mice, the specific microbial species driving these downstream alterations remained unclear. Given that *E. avium* abundance was strongly correlated with HIC symptom scores (Fig. 4G), associated with high mortality rates, capable of influencing bile acid metabolism, and even isolated from bile fluid[22,23], we hypothesized that *E. avium* induce urothelial injury through upregulation of TCDCA. To test this, *E. avium* was transplanted into Abx-mice via oral gavage every other day for two weeks (Fig. 6A). Metagenomic sequencing revealed a significant increase in *E. avium* abundance, indicating successful colonization in recipient mice (Fig. 6B). Following transplantation, mice exhibited the increased urinary frequency (Fig. 6C) and reduced pain threshold (Fig. 6D). Histological analysis showed the decreased expression of ZO-1 and increased expression of TNF-α and TLR3 in the bladder (Fig. 6E). Following *E. avium* transplantation, targeted BA analysis revealed a concurrent and consistent elevation of TCDCA and TUDCA levels in both mice blood and urine, whereas levels of other BAs remained unchanged or showed inconsistent alterations between the two compartments (Fig. 6F, G; Supplementary Tables 5, 6). These findings demonstrate that *E. avium* transplantation might induce BA dysregulation and aggravate bladder injury in recipient mice, supporting its role as a key microbial contributor in HIC pathogenesis.

We next investigated whether TCDCA or TUDCA directly induces bladder injury. Previous studies have reported the cytotoxic properties of TCDCA[19], suggesting it may act as a risk factor, whereas TUDCA is a well-established inhibitor of endoplasmic reticulum stress and is known to support inflammatory homeostasis and metabolic regulation[20]. To test their direct effects on the urothelium, we treated human urothelial cells (HUCs) with varying concentrations of TCDCA and TUDCA. TCDCA at 200 μM significantly reduced cell viability, while TUDCA exhibited no cytotoxic effects (Fig. 6H and Supplementary Table 7). Additionally, TCDCA disrupted tight junctions, upregulated TNF-α expression, and activated TLR3 signaling (Fig. 6I).

Considering that urinary TCDCA comes into direct contact with the urothelium, we further performed intravesical instillation of TCDCA in rats to evaluate its in vivo effects (Fig. 6J), as bladder instillation in mice is technically challenging. The results showed that TCDCA increased voiding frequency (Fig. 6K), lowered the pain threshold (Fig. 6L), and aggravated bladder pathology (Fig. 6M and

https://doi.org/10.1038/s41467-025-68060-1

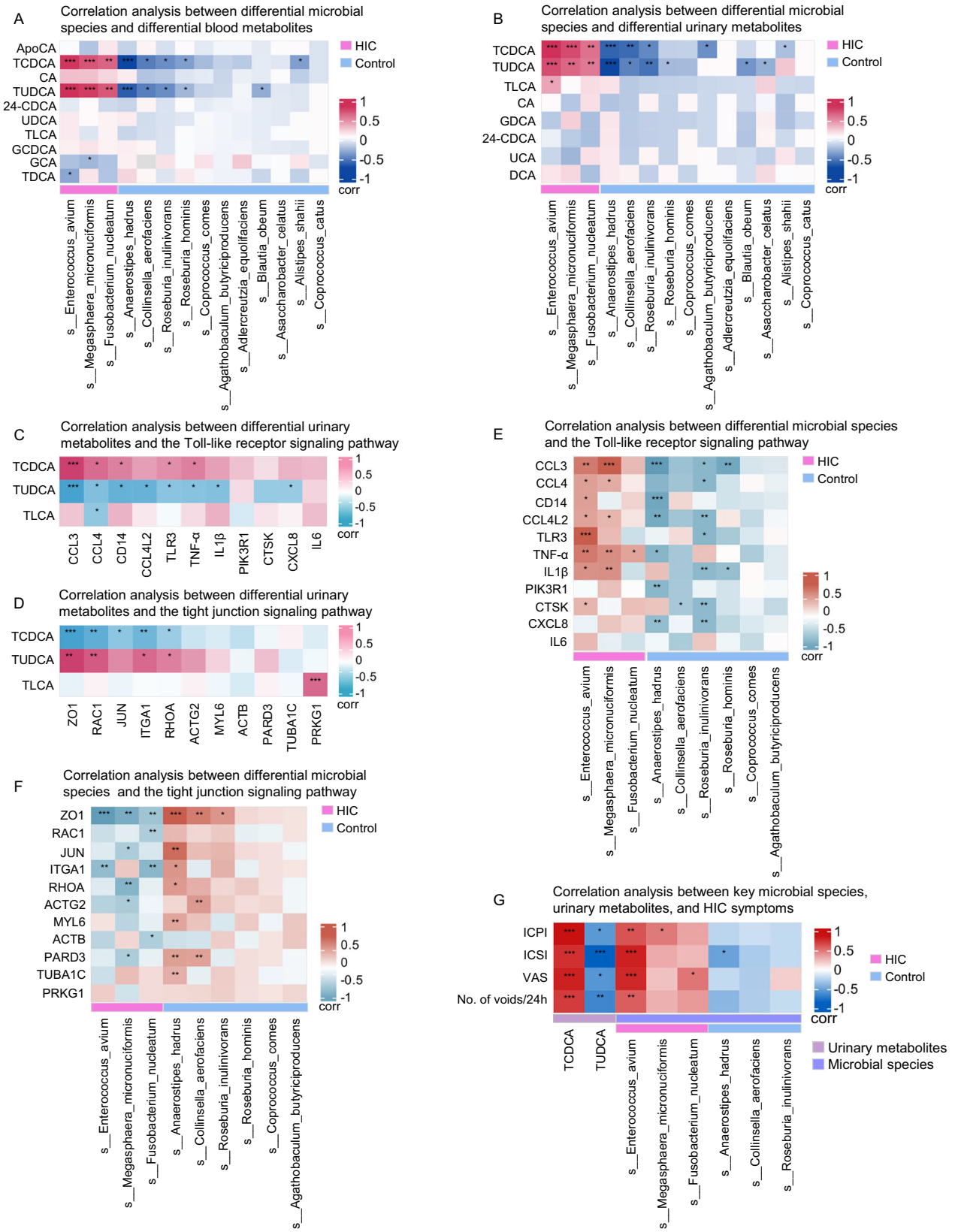

Fig. 4 | Crosstalk among gut microbiota alterations, bile acid metabolism, and bladder injury-related pathways in HIC. Spearman correlation between differential microbial species and altered blood (**A**) and urinary (**B**) metabolites (No. matched participants, $n = 60$). Correlation between differential urinary metabolites and gene expression in the Toll-like receptor (**C**) and cell junction (**D**) signaling pathways based on single-cell RNA sequencing (No. matched participants, $n = 17$). Correlation between differential microbial species and genes involved in the Toll-like receptor (**E**) and cell junction (**F**) signaling pathways (No. matched participants, $n = 17$). **G** Spearman correlation of key microbial species and urinary metabolites with clinical symptom scores, including interstitial cystitis symptom index (ICSI), problem index (ICPI), and visual analogue scale (VAS) (No. matched participants, $n = 60$). Statistical analysis: two-sided Spearman correlation was used for all panels (**A**–**G**). $^{*}p < 0.05$; $^{**}p < 0.01$; $^{***}p < 0.001$. Source data are provided as a Source Data file.

Supplementary Fig. 2E), thereby confirming its detrimental impact on bladder function.

In conclusion, through *E. avium* transplantation, we demonstrated that *E. avium* may induce the upregulation of TCDCA, which directly disrupts cell junction integrity, activates inflammation, and triggers TLR3 signaling in HIC.

TCDCA-mediated urothelial injury via TLR3 signaling

The results from single-cell transcriptomics, FMT, and TCDCA instillation highlighted the crucial role of TLR3 signaling in mediating HUC barrier function and inflammation. To further investigate its involvement in TCDCA-induced HUC injury, we treated HUCs pretreated with 200 μM TCDCA with either a TLR3 agonist (Poly(I:C)) or inhibitor (TLR3 siRNA I). Our findings showed that Poly(I:C) exacerbated HUC inflammation and maintained barrier damage, while the TLR3 inhibitor restored tight junction integrity and reduced inflammation (Fig. 7A–C). Additionally, we tested pentosan polysulfate sodium (PPS), the only FDA-approved medication for treating IC/BPS[24], as a potential therapeutic agent for rescuing TCDCA-induced HUC injury. PPS treatment led to upregulation of ZO-1 expression and downregulation of TLR3 and TNF-α expression (Fig. 7D, E). Moreover, transepithelial resistance (TER) was significantly improved following PPS treatment (Fig. 7F). Similarly, both the TLR3 inhibitor (CU-CPT 4a) and PPS were administered to rats that received intravesical instillation of TCDCA (Fig. 7G). These treatments decreased urination frequency, increased pain threshold (Fig. 7H), and alleviated bladder pathological changes (Fig. 7I and Supplementary Fig. 2F).

Taken together, by integrating metagenomics, targeted metabolomics, and single-cell transcriptomics, we uncovered a novel microbial–metabolic–immune axis involving *E. avium*, TCDCA, and TLR3, which appears to mediate urothelial barrier injury in HIC. The findings offer novel insights into the gut–bladder axis and expand the current understanding of HIC from a multi-systemic perspective. To our knowledge, this is the first study to implicate *E. avium* and BA metabolism, particularly TCDCA, in the activation of bladder inflammation via innate immune activation. Functional validation in animal and cellular models further supports the role of the *E. avium*–TCDCA–TLR3 axis in disease pathogenesis, highlighting potential targets for future therapeutic intervention.

Discussion

Although HIC is clinically defined by bladder-centric symptoms, accumulating evidence suggests systemic involvement. Prior investigations explored alterations in the microbiome, transcriptome, and metabolome across different biological compartments. However, the lack of resolution in earlier techniques and limited cross-platform integration have constrained mechanistic insights. In this study, we sought to overcome these challenges by leveraging a multi-omics framework—combining metagenomics, targeted metabolomics of urine and plasma, and single-cell transcriptomics—to better delineate the molecular pathways contributing to urothelial injury in HIC. The results revealed that *E. avium*, *M. micronuciformis*, and *F. nucleatum* were significantly upregulated at the species level, suggesting their potential as biomarkers for HIC (AUC: 0.881). The functions of these differentiated microbial species were closely associated with BA metabolism. Metabolomic analysis of serum and urine identified that key metabolites were enriched in BA metabolism, with concurrent elevation of TCDCA and TUDCA in both serum and urine of HIC patients. Single-cell transcriptomic analyses further supported that TLR3 signaling mediates urothelial injury. Multi-omics correlation network analysis proposed an *E. avium*–TCDCA–TLR3 axis as a contributing factor to LUTS. FMT from HIC patients confirmed increased urinary TCDCA and TUDCA levels and aggravated bladder injury in Abx-mice. *E. avium* transplantation experiments validated that *E. avium* induced urothelial injury through TCDCA upregulation. Both in vivo and in vitro studies demonstrated that TCDCA directly disrupts cell junction integrity and activates inflammation via TLR3 signaling in HIC.

Growing evidence supports the autoimmune component of human IC/BPS, particularly in HIC subtypes characterized by immune dysregulation and chronic inflammation[25]. The AC model, generated through bladder tissue homogenate immunization, recapitulates key pathological and clinical features of HIC, including urothelial barrier disruption, mast cell infiltration, elevated proinflammatory cytokines, and bladder hyperalgesia[26–28]. These hallmarks closely parallel the histological and symptomatic manifestations observed in patients. Thus, the AC model provides a clinically relevant platform to dissect immune-mediated mechanisms and evaluate potential therapeutic targets, which justified its selection in the present study. However, given the ongoing uncertainty regarding the precise etiology of IC/BPS, it is important to note that this inflammatory model serves primarily as a surrogate for the injured state of the urothelium. Notably, our findings suggest that TCDCA may itself represent a direct inducer of urothelial injury, warranting further investigation as a potential alternative modeling approach in future studies.

Previous studies from our group have suggested that UCs may be the primary target of injury in IC/BPS, with altered cell communication playing a central role, as demonstrated by single-cell RNA sequencing and spatial transcriptomics[4,29]. Specifically, a reduction in UC proportions, along with increased communication between urothelial and other cell types in the bladder, implies that urothelial injury is a critical pathological process in HIC[5]. This finding aligns with recent work characterizing the immune microenvironment in HIC[30]. Future research should therefore focus on identifying the upstream mechanisms driving urothelial injury.

To investigate the upstream causes of urothelial injury, we performed the first metagenomic analysis of the gut microbiota in HIC patients, which revealed microbial composition shifts linked to bile acid metabolism and identified *E. avium*, *M. micronuciformis*, and *F. nucleatum* as potential diagnostic biomarkers. Despite the inherent complexity of HIC diagnosis, the diagnostic specificity (AUC: 0.881) achieved by these three species surpasses that of traditional urinary biomarkers[13] such as IL-6 (AUC: 0.731)[31] and methylhistamine (AUC: 0.644)[31]. *E. avium*, commonly associated with multi-microbial infections like splenic abscesses[21], cholecystitis[22], and bacteremia[23], has been linked to high mortality rates and can be isolated from bile fluid[22]. This further supports the potential relationship between *E. avium* and bile acid metabolic dysfunction.

Although patients with IC/BPS show a higher prevalence of metabolic syndrome[32], recent studies have identified lipid acids[7,9] and amino acids[12,33] as the dominant factor in this disorder. However, the role of BA metabolism in IC/BPS remains underexplored. Notably, a previous study emphasized the involvement of the BA receptor TGR5 in bladder afferent hypersensitivity[15], suggesting a potential mechanistic link between BA metabolism and IC/BPS pathology. Notably, TCDCA, a BA known for its cytotoxic effects, induces mitochondrial permeability transition and Caspase-11-mediated pyroptosis in hepatocytes[19]. In our study, we demonstrated that TCDCA similarly causes urothelial injury in HUCs via TLR3 activation, which had not been previously explored.

A methodological limitation of this study is the difference in urine collection methods between controls and HIC patients. Midstream clean-catch urine was used for controls, while transurethral catheterization was performed for HIC patients to ensure sufficient and consistent sample volumes due to their severe urinary urgency and pain. This discrepancy may introduce variability in metabolomic profiles, and future studies with harmonized collection methods are warranted to further validate these findings.

In conclusion, our integrative multi-omics approach identifies the *E. avium*–TCDCA–TLR3 axis as a potential contributor to the

https://doi.org/10.1038/s41467-025-68060-1

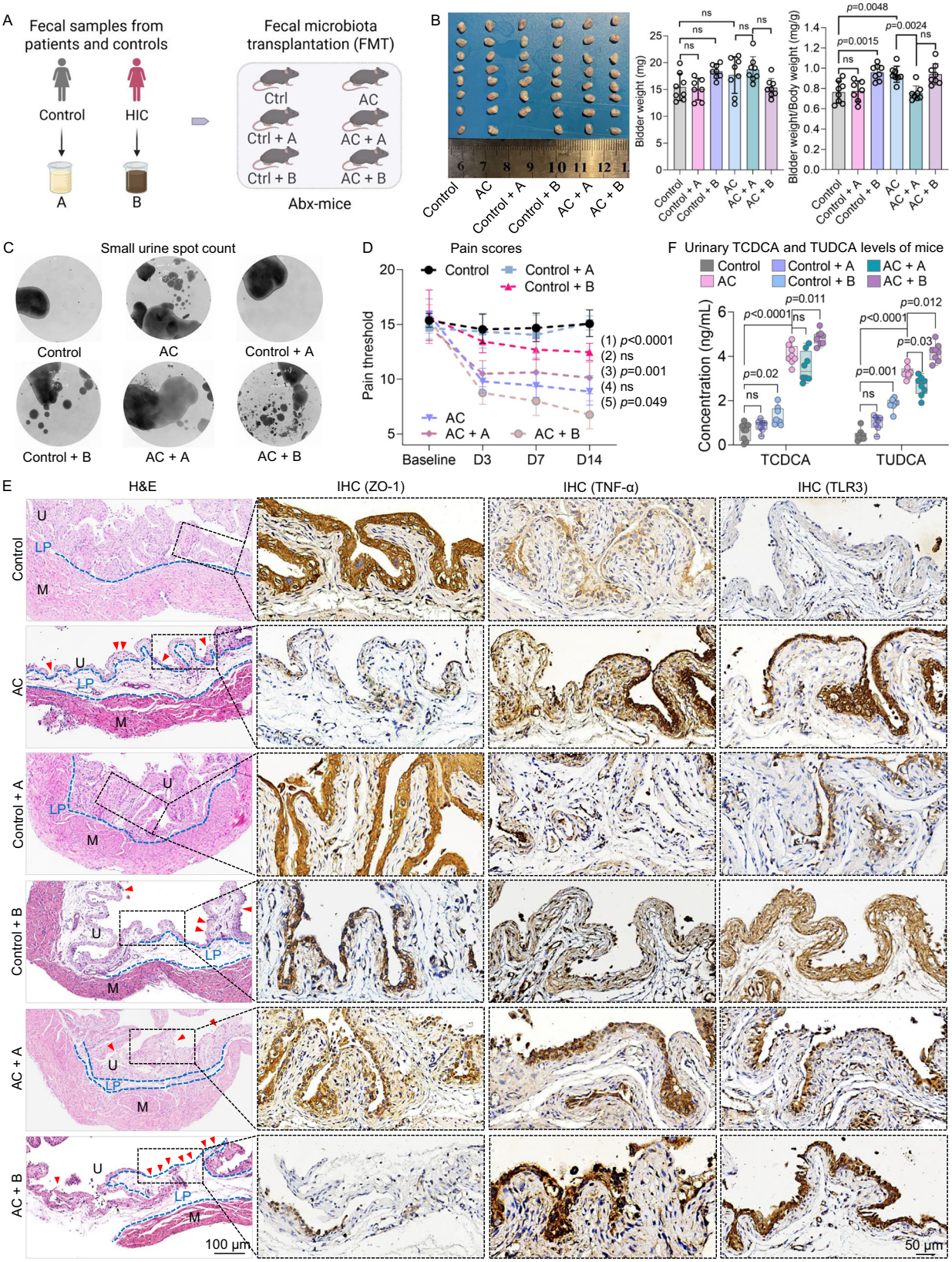

pathogenesis of HIC. Functional validation through FMT, bacterial transplantation, metabolite instillation, and cellular and animal models supports the involvement of TLR3 signaling in TCDCA-induced urothelial injury. While further studies are warranted, these findings may aid in refining diagnostic approaches and provide a foundation for individualized therapeutic strategies in IC/BPS.

Methods

Study population

The diagnosis of Hunner-type IC/BPS was made by the same urologist based on the NIDDK guideline[34]. Female patients meeting the inclusion and exclusion criteria (Supplementary Table 2) were enrolled. Hunner lesions in patients with HIC were identified through cystoscopy. Full-

Fig. 5 | HIC-derived fecal microbiota alters host metabolism and increases bladder vulnerability. A Fecal microbiota transplantation (FMT) in antibiotic-pretreated mice (Abx-mice), using stool samples from healthy controls (Group A, No. of controls = 5) and HIC patients (Group B, No. of patients = 5). **B** Bladder weight comparison post-FMT. **C** Assessment of voiding behavior in FMT-recipient mice (each mouse measured once). **D** Evaluation of mechanical pain threshold following FMT. Comparisons: (1) Control vs. Autoimmune cystitis (AC); (2) Control vs. Control + A; (3) Control vs. Control + B; (4) AC vs. AC + A; (5) AC vs. AC + B. **E** Representative histological analysis of bladder tissues after FMT (one section and field per mouse). **F** Quantification of urinary TCDCA and TUDCA in recipient mice. For panels (**B**–**F**): group sizes are $n = 7$ for Control + A and $n = 8$ for all other groups; data are presented as median (IQR); statistical analysis was performed using the Kruskal–Wallis test; ns not significant. IHC immunohistochemistry, Red arrow: urothelial thinning, detachment, and exposure, Blue line: LP lamina propria, U urothelium, M muscularis. Source data are provided as a Source Data file.

thickness bladder tissue from HIC patients was obtained via transurethral resection prior to hydrodistension.

Healthy women undergoing routine health examinations at our institute served as controls. All participants were female and free from urological malignancies, stones, infections, or malformations. Individuals with a history of liver or thyroid disease, COPD, radiotherapy, or chemotherapy were excluded. Additional exclusion criteria included recent (within 3 months)[8,35] use of antibiotics, probiotics, prebiotics, synbiotics, or other medications, as well as the presence of metabolic disorders, hypertension, or diabetes. Participants with chronic diarrhea or constipation or a history of gastrointestinal surgery were also excluded. Stool[6], blood[35], urine[8], and bladder tissue samples[5] were collected as previously described with modifications for 16S rRNA, metagenomic, metabolomic, and single-cell transcriptional analyses. For single-cell transcriptional analysis of control bladder tissue, female patients with pure stress urinary incontinence (PSUI) and stable bladder function undergoing anti-incontinence surgery were included[4,10].

Symptoms were evaluated using daily voiding frequency, nocturia episodes, the O'Leary-Sant Interstitial Cystitis Symptom Index (ICSI), the Interstitial Cystitis Problem Index (ICPI), and a 10-point visual analog scale (VAS)[4].

Ethical approval (#2019186) was obtained from West China Hospital, and informed consent was obtained from all candidates before the study.

Sample collection

The sample collection was performed according to the methodologies described in previous literature[4,6,8,10,35]. Approximately 5–7 mL of venous blood was collected from each subject[35]. The urinary meatus and perineum of all participants were disinfected using a 0.5% iodophor solution. A 50 mL sample of clean midstream urine was collected from each control participant, while the midstream urine of each patient diagnosed with HIC was collected using transurethral catheterization and collected into a sterile 50 mL container[8,10,35,36]. Blood samples: After collection, blood was centrifuged at 3000 × *g* for 10 min at 4 °C to separate serum. Urine samples: Fresh urine was immediately centrifuged at 15,000 × *g* for 10 min at 4 °C to remove cells, crystals, and debris.

Fecal samples were collected from all participants at the time of enrollment using sterile collection containers. Samples were immediately stored at −80 °C until DNA extraction and gut microbiota analysis[6].

HLs in patients with HIC were identified through cystoscopy, and then full-thickness bladder samples from patients with HIC were obtained through transurethral resection of the bladder prior to hydrodistension. Full-thickness control bladder samples from patients with PSUI[4] were collected through transurethral resection of the bladder after sling procedures during bladder injury assessment. Bladder tissue samples are preserved in a specific tissue preservation solution and transported to the laboratory on ice within 30 min.

Despite our best efforts to collect all biospecimen types from each patient, limited sample volumes, occasional assay failures, and quality control exclusions have led to discrepancies in sample availability across patients, resulting in unmatched sample numbers for different analyses.

16S rRNA and shotgun metagenomic sequencing

16S rRNA sequencing was performed on fecal samples from 32 Hunner-type IC/BPS patients and 30 healthy controls, following previously established protocols[37]. The V3–V4 hypervariable regions of the bacterial 16S rRNA gene were amplified using primers 338F and 806R on a GeneAmp 9700 PCR system. Sequencing was conducted on an Illumina MiSeq PE300 platform (Illumina, San Diego, USA) according to the standard protocols of Majorbio Bio-Pharm Technology Co. Ltd. (Shanghai, China). Alpha diversity indices (Chao, ACE, Shannon, Simpson) were calculated to assess within-sample diversity, and the coverage index was used to evaluate sequencing depth. Beta diversity (inter-individual variation) was analyzed via principal coordinates analysis (PCoA) and the Adonis test. Differentially abundant taxa between groups were identified using Linear Discriminant Analysis Effect Size (LEfSe).

To achieve species-level resolution, shotgun metagenomic sequencing was also performed on fecal DNA from the same participants. Briefly, DNA was fragmented to an average size of ~400 bp for paired-end library construction using the NEXTFLE Rapid DNA-Seq kit[38]. Sequencing was carried out on the Illumina NovaSeq 6000 platform (Illumina Inc., San Diego, CA, USA). Metagenomic functional annotation was performed using HUMAnN3 with the ChocoPhlAn database for human samples, and DIAMOND (v2.0.13) against the NCBI NR protein database (version 20230830) for mouse samples. Then, functional analysis of differential microorganisms in the two groups was performed. All 16S rRNA and metagenomic data were processed using the Majorbio Cloud Platform (www.majorbio.com).

Non-targeted metabolomics

Metabolomic analyses of blood and urine samples from 50 Hunner-type IC/BPS patients and 30 healthy controls were performed at Shanghai Applied Protein Technology Co. Ltd. (Shanghai, China). For both sample types, 100 μL of supernatant was then mixed with 400 μL of ice-cold methanol/acetonitrile (1:1, v/v) to precipitate proteins, followed by vortexing and a second centrifugation at 15,000 × *g* for 15 min at 4 °C. The resulting supernatant was collected for LC-MS/MS analysis. Using a UHPLC system (1290 Infinity LC, Agilent Technologies) coupled with a quadrupole time-of-flight mass spectrometer (TripleTOF 6600, AB Sciex), as previously described[39]. Processed data were normalized and subjected to multivariate analysis, including Pareto-scaled principal component analysis (PCA) and orthogonal partial least-squares discriminant analysis (OPLS-DA). Variable importance in projection (VIP) score was calculated from the OPLS-DA model to evaluate each metabolite's contribution to group separation. Metabolites with VIP ≥ 1 and $p < 0.05$ were considered statistically significant. Functional prediction of differentially abundant metabolites was performed using the Kyoto Encyclopedia of Genes and Genomes (KEGG) database.

Targeted bile acid (BA) analysis

BAs in the extracted samples were separated using an ACQUITY BEH C18 column (1.7 μm, 100 × 2.1 mm; Waters, Milford, MA). Quantification was performed by LC-MS/MS on an ACQUITY UPLC system coupled

https://doi.org/10.1038/s41467-025-68060-1

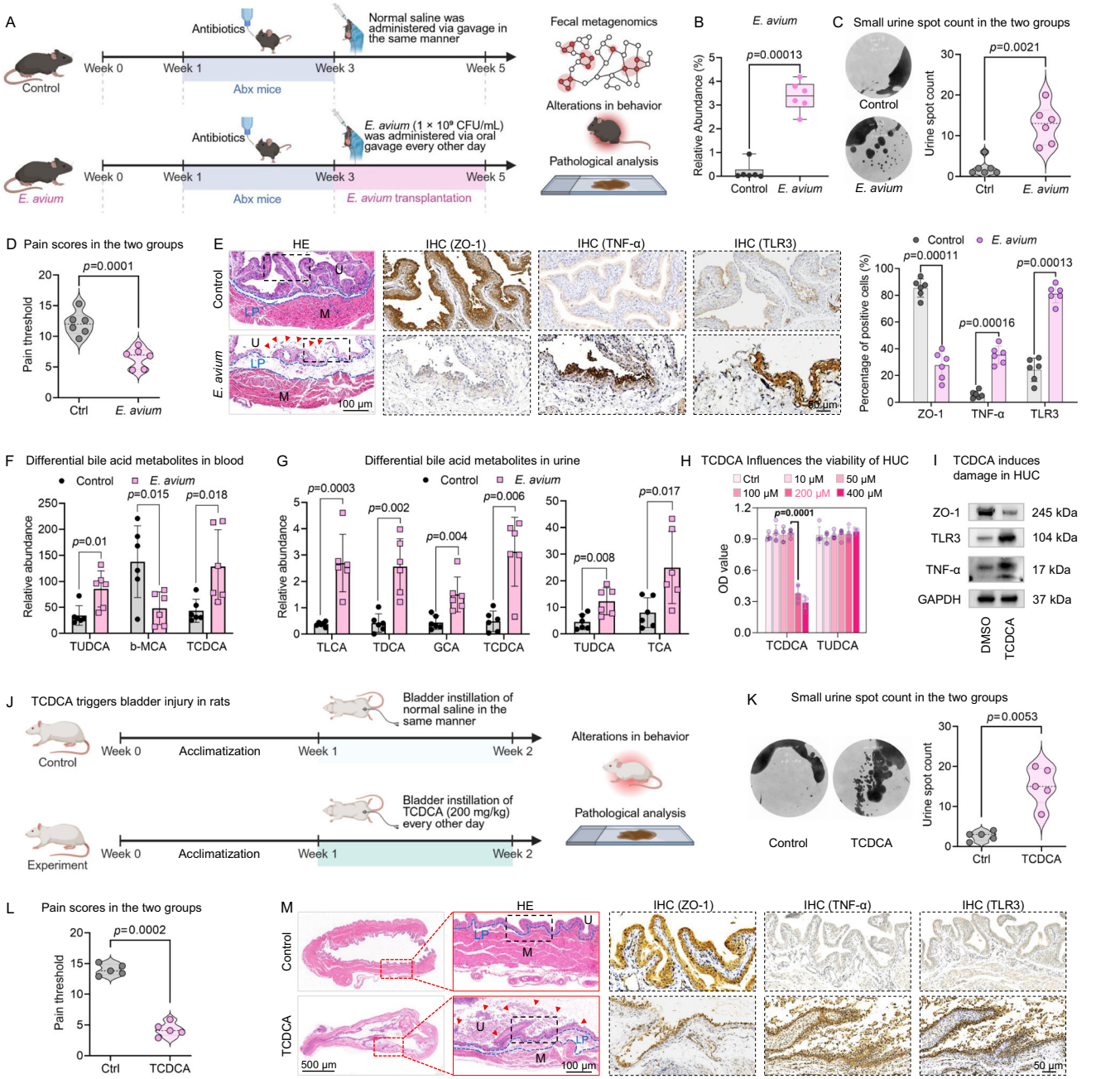

Fig. 6 | *E. avium* transplantation induces urothelial injury via TCDCA upregulation. A Experimental workflow of *E. avium* colonization in antibiotic-pretreated mice (Abx-mice, $n = 6$ per group). Created in BioRender. Chen, J. (2025) https://BioRender.com/3lccwo1. **B** Increased abundance of *E. avium* confirmed by metagenomic sequencing ($n = 6$ per group). **C** Evaluation of voiding behavior following *E. avium* transplantation ($n = 6$ per group; one measurement per mouse). **D** Measurement of mechanical pain threshold post-transplantation ($n = 6$ per group). **E** Representative histological analysis of bladder tissues after *E. avium* transplantation ($n = 6$ per group; one section and field per mouse). **F**, **G** Quantification of blood and urinary bile acids using comprehensive targeted bile acid profiling ($n = 6$ per group). **H** Cell viability of human urothelial cells (HUCs) following TCDCA or TUDCA treatment ($n = 3$ independent experiments). **I** Expression of ZO-1, TNF-α, and TLR3 following TCDCA (200 μM) exposure ($n = 3$ independent experiments). **J** Experimental workflow of intravesical instillation of TCDCA in rats ($n = 5$ per group). Created in BioRender. Chen, J. (2025) https://BioRender.com/3lccwo1. **K** Evaluation of voiding function after TCDCA instillation ($n = 5$ per group; each rate measured once). **L** Assessment of mechanical pain threshold following TCDCA exposure ($n = 5$ per group). **M** Representative histology of bladder tissues post-instillation ($n = 5$ per group; one section per rat, one field quantified per section). For panels (**B**–**H**, **K**, **L**): data are presented as median (IQR). Statistical analysis was performed using the two-sided Mann–Whitney *U* test. IHC immunohistochemistry, Red arrow: urothelial thinning, detachment, and exposure, Blue line: LP lamina propria, U urothelium, M muscularis. Source data are provided as a Source Data file.

with a XEVO TQ-S mass spectrometer equipped with an electrospray ionization source. A standard mixture of BAs was analyzed at regular intervals, and concentrations of individual BAs were calculated based on corresponding standard curves derived from raw UPLC-MS data[40,41]. LC-MS/MS analysis was technically supported by Shanghai Applied Protein Technology Co. Ltd. (Shanghai, China).

RNA sequencing

RNA sequencing was performed following standard protocols[42]. Raw data were retrieved from the GEO database, including HIC samples (accession number GSE238208) and control samples (accession number GSE11783). All datasets were normalized before analysis. All datasets were normalized before analysis. Differentially expressed

https://doi.org/10.1038/s41467-025-68060-1

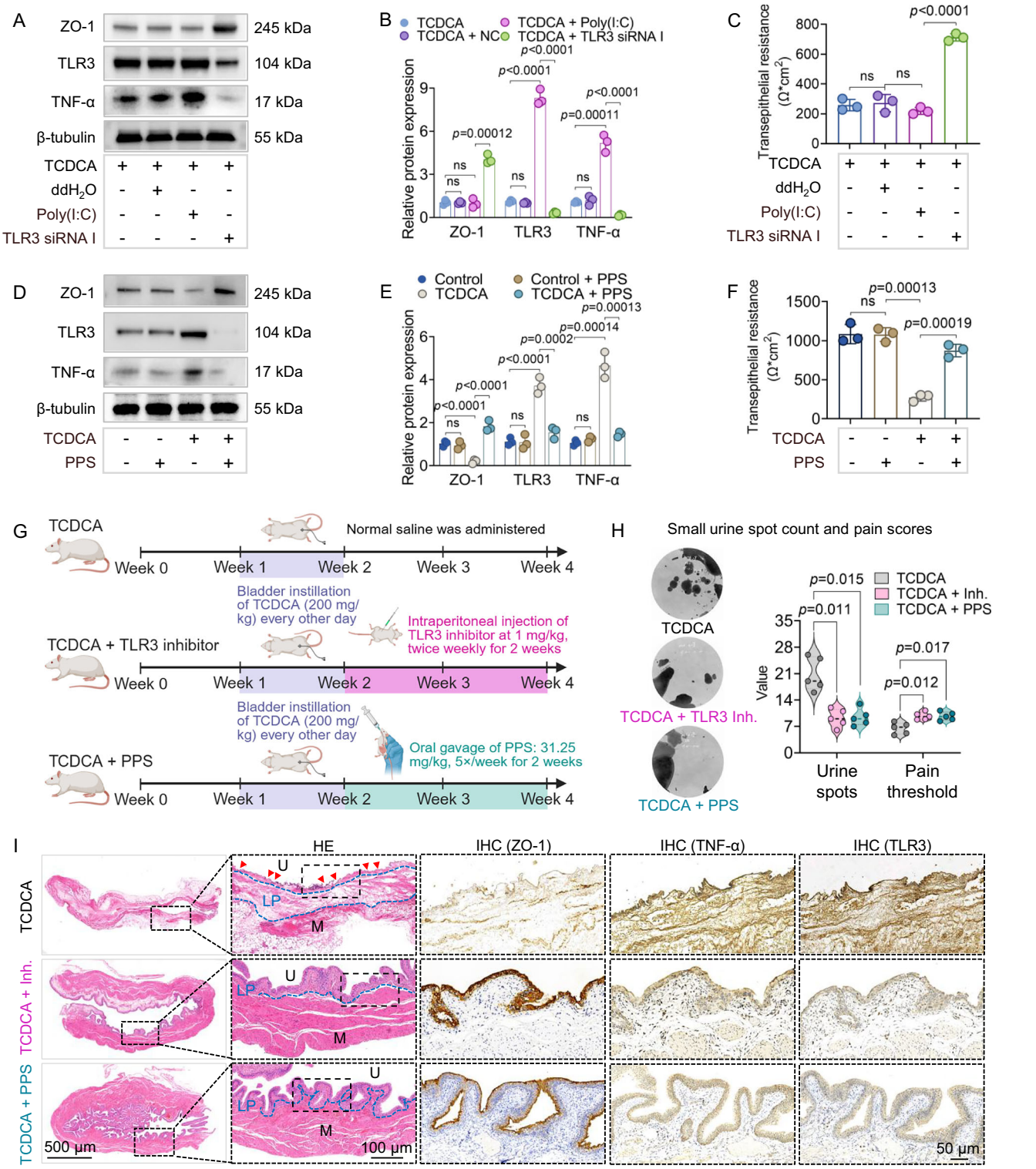

Fig. 7 | TCDCA-induced urothelial injury via TLR3 signaling. A, **B** Expression of tight junction protein ZO-1 and inflammatory marker TNF-α after TLR3 intervention in TCDCA-pretreated human urothelial cells (HUCs) ($n = 3$ independent experiments). **C** Transepithelial resistance (TER) changes following TLR3 intervention in TCDCA-pretreated HUCs ($n = 3$ independent experiments). **D**, **E** Expression of ZO-1 and TNF-α after pentosan polysulfate sodium (PPS) administration in TCDCA-pretreated HUCs ($n = 3$ independent experiments). **F** TER changes following PPS intervention in TCDCA-pretreated HUCs ($n = 3$ independent experiments). **G** Experimental workflow showing TLR3 inhibitor and PPS administration to rats following intravesical TCDCA instillation ($n = 5$ per group). Created in BioRender. Chen, J. (2025) https://BioRender.com/3lccwo1. **H** Assessment of voiding function (one measurement per rat) and pain threshold after TLR3 inhibition ($n = 5$ per group). **I** Representative histological images of bladder tissues post-TLR3 inhibition ($n = 5$ per group; one section and field per rat). For panels (**B**, **C**, **E**, **F**, **H**): data are presented as median (IQR). Statistical analysis was performed using the Kruskal–Wallis test. ns not significant, IHC immunohistochemistry, Red arrow: urothelial thinning, detachment, and exposure, Blue line: LP lamina propria, U urothelium, M muscularis. Source data are provided as a Source Data file.

genes (DEGs) between groups were identified using an adjusted *p*-value < 0.05 and $|\log_2$ fold change$|\geq 2$. Gene Ontology (GO) and pathway enrichment analyses were conducted based on DEGs, with significance determined by a false discovery rate threshold of <0.05.

Single-cell RNA sequencing

Single-cell suspension preparation, library construction, and data analysis were conducted as described in our previous study[4,5]. Urothelial cells (UCs) were identified based on canonical markers *KRT19* and *UPK1A* from 10 Hunner-type IC/BPS patients and 7 PSUI controls[5]. DEGs between Hunner-type IC/BPS and control groups were identified using a threshold of adjusted $p < 0.05$ and |lg fold change|≥0.5. GO and KEGG enrichment analyses were performed on the DEGs. Additionally, Gene Set Enrichment Analysis (GSEA) was applied to explore altered pathways in UCs.

Construction of correlation network

Spearman correlation analyses were conducted using R software (version 3.6.1: https://www.r-project.org) to evaluate the relationships between the microbiome, metabolomics, single-cell transcriptomics, and clinical symptoms[43]. Significant associations in the interaction networks were defined as those with statistically significant *p*-values ($p < 0.05$).

Antibiotic-treated mice (Abx-mice)

All mouse experiments were approved by the Animal Care and Use Committee of Sichuan University (No. 20221115001). Female C57BL/6 mice (6 weeks old, $n = 48$) were purchased from Dossy Experimental Animal Co., Ltd. (Chengdu, China) and housed in a specific pathogen-free facility under a 12 h light/12 h dark cycle with ad libitum access to a standard diet. Mice were group-housed (four per cage) and acclimatized with a standard diet for one week prior to treatment. To establish the Abx- mouse model, mice received a cocktail of broad-spectrum antibiotics in their drinking water for two weeks[44], including ampicillin (1 g/L), neomycin (1 g/L), metronidazole (1 g/L), vancomycin (0.5 g/L), and amphotericin B (10 mg/L).

Autoimmune animal model of HIC

The autoimmune cystitis (AC) HIC model was established with modifications based on a previously reported protocol[26–28]. Briefly, an antigen solution was prepared from the bladder tissues of healthy C57BL/6 mice at a final concentration of 1 mg/mL. After one week of acclimatization, mice received a subcutaneous injection of 400 µL of the antigen solution, followed by a second injection of the same dose one week later.

Fecal microbiota transplantation (FMT)

Stool samples were randomly collected and pooled from 5 healthy controls (Group A) and 5 patients with Hunner-type IC/BPS (Group B)[41]. A total of 200 milligrams of feces were resuspended in 1 mL of sterile anaerobic PBS. Following resuspension, the mixture was centrifuged at 800 × *g* for 3 min. The resulting supernatant was then passed through a 70-µm filter to eliminate large particulate matter, while the suspended pellets were stored at −80 °C[45]. At 9 weeks of age, the mice in the following groups: Control + A (Abx-mice transplanted with stool samples from healthy controls without antigen solution injection), Control + B (Abx-mice transplanted with stool samples from HIC patients without antigen solution injection), AC + A (Abx-mice transplanted with stool samples from healthy controls with antigen solution injection), and AC + B (Abx-mice transplanted with stool samples from HIC patients with antigen solution injection) were orally inoculated with 200 µL of the prepared fecal suspension three times daily for 2 weeks[45]. Recipient mice, who received the microbiota transplantation, were housed in separate Trexler-type film isolators, and provided with sterile food and water to strictly control bacterial contamination. Their body weights, voiding behaviors, and pain scores were recorded at 3, 7, and 14 days. After 14 days, the mice were euthanized by carbon dioxide (CO_2) inhalation followed by cervical dislocation, and bladder, blood, and urine samples were collected as much as possible for pathological experiments and metabolite detection.

Voiding behavior assessments

Voiding behavior was evaluated following a previously described protocol[5]. Each mouse was placed in an individual cage to acclimate to the new environment for one hour. Subsequently, a sheet of filter paper (Whatman, Cat. 1540-125) was placed on the cage floor, and the mice were observed for one hour after the suspension of water and diet. The filter paper was then photographed under ultraviolet light, and the number of urine spots with a diameter <0.2 cm^2 was recorded. A higher number of spots indicated a greater frequency of urinary episodes.

Pain threshold detection

Pain threshold[5] was assessed using an electronic von Frey anesthesiometer (IITC, Inc., USA). The mice were housed in transparent cages with a wire grid floor. After 30 min of environmental adaptation, a gradually increasing vertical force was applied to the central area of the pelvic region using the tip of the electronic von Frey anesthesiometer. The instrument automatically recorded the intensity of the force when it elicited avoidance behaviors in mice. The pain threshold value for each mouse was determined as the average of three measurements.

Pathological staining and immunohistochemistry (IHC)

The samples were fixed overnight in 4% paraformaldehyde, embedded in paraffin, and sliced into 5 µm sections. The sections were subjected to H&E staining to examine the general morphology. Immunohistochemical staining was performed using primary antibodies against TLR3 (Abcam, Cat. ab62566 or Affinity, Cat. DF6415), TNF-α (Affinity, Cat. AF7014), and ZO-1 (Proteintech, Cat. 21773-1-AP). The primary antibody was detected using a biotinylated secondary antibody, and visualized using the VECTASTAIN ABC peroxidase system and peroxidase substrate DAB kit. The expression levels of TLR3, ZO-1, and TNF-α proteins were assessed at 100 × magnification in five different fields of view using Image-Pro Plus (version 6.0).

Enterococcus avium (E. avium) transplantation

E. avium was isolated from fecal samples using selective culture conditions and identified based on colony morphology, Gram staining, and 16S rRNA gene sequencing. All procedures were performed following previously described protocols[46]. Twelve Abx-treated mice were randomly divided into two groups: a normal control group and an *E. avium* group. In the *E. avium* group, mice were orally gavaged with 1×10^9 CFU/mL of *E. avium* every other day for two weeks, while the control group received an equal volume of normal saline following the same schedule. After two weeks, the mice were euthanized, and stool metagenomic sequencing, behavioral assessment, bladder pathological analysis, and targeted bile acid analysis of blood and urine samples were performed as described above.

Human urothelial cell (HUC) culture

Primary bladder urothelial cells (ATCC, Cat. PCS-420-010) were cultured in bladder epithelial cell basal medium (ATCC, Cat. PCS-420-032) supplemented with bladder epithelial growth kit (ATCC, Cat. PCS-420-042) at 37 °C in a humidified atmosphere of 95% air and 5% CO_2. HUCs were cultured for three to seven generations, demonstrating normal morphology and a stable state. Subsequently, the cells were transferred to a six-well plate to proceed with the subsequent experiments.

TLR3 and PPS intervention in a TCDCA-induced injury model

HUCs were treated with varying concentrations of taurochenodeoxycholic acid (TCDCA, MCE, Cat. HY-N2027) or tauroursodeoxycholic acid (TUDCA, MCE, Cat. HY-19696) for 24 h, followed by a CCK-8 assay to assess cytotoxicity. Based on the results, exposure to 200 μM TCDCA for 24 h was selected to establish the in vitro injury model. Control cells were maintained under identical conditions without treatment.

To explore the role of Toll-like receptor 3 (TLR3), TCDCA-pretreated HUCs were treated with either a TLR3 agonist (Poly(I:C) Sodium Salt, CST, Cat. 61401; 5 μg/mL) or TLR3 siRNA (Toll-like Receptor 3 siRNA I, CST, Cat. 6236; 100 nM). Additionally, pentosan polysulfate sodium (PPS, Selleck, Cat. S3500; 200 μg/mL)[5] was applied to the TCDCA-induced injury model to evaluate its therapeutic effect. PPS is the only oral treatment approved by the US FDA for IC/BPS[24]. The integrity of the cellular barrier, assessed by measuring the expression of ZO-1 and transepithelial resistance[5], as well as the level of inflammation, determined by TNF-α expression[5], were evaluated in these experimental groups. The primer sequences for the genes mentioned above are listed in Supplementary Table 7.

Western blotting

HUCs were homogenized in RIPA lysis buffer supplemented with complete protease inhibitors and phosphatase inhibitor. The protein lysates were then boiled with 5× SDS-buffer at 99 °C for 10 min. Subsequently, the samples were separated on 4–20% SDS-PAGE gels and transferred to a PVDF membrane. The PVDF membrane was blocked with 5% BSA and incubated overnight at 4 °C with the following primary antibodies: anti-beta tubulin (Affinity, Cat. T0023), anti-GAPDH (Affinity, Cat. AF7021), anti-TLR3 (Abcam, Cat. ab62566), anti-TNF-α (Affinity, Cat. AF7014), or anti-ZO-1 (Abcam, Cat. ab216880). After incubation, the membrane was further incubated for 1 hour with appropriate secondary antibodies (ZENBIO, Cat: 511203 or 550017). Protein bands were visualized using Immobilon Western Chemiluminescent HRP Substrate (Merck Millipore, Billerica, MA, USA). Densitometry analysis was performed using ImageJ software (National Institutes of Health, Bethesda, USA).

Transepithelial resistance

As previously mentioned[5], HUCs were seeded onto the upper level of Transwell chambers and cultured until they formed a confluent monolayer on the filter membrane. The culture medium was regularly replaced to ensure cell growth and maturation. Subsequently, we assessed the changes in cellular transmembrane resistance using a RE1600 resistograph. The tight intercellular junctions formed by the cells on the filter membrane contribute to the overall resistance, reflecting their barrier function.

TCDCA-induced bladder injury model in rats

All rat experiments were approved by the Animal Care and Use Committee of Sichuan University (No. 20251203004). Twenty 6-week-old female Sprague-Dawley rats were randomly assigned to four groups. Rats were housed under specific pathogen-free conditions at 22 ± 2 °C with 50–60% humidity and a 12-h light/dark cycle, with ad libitum access to food and water. After one week of acclimatization, the following interventions were performed: Control group: Intravesical instillation of normal saline every other day for 1 week (1 h per session). TCDCA group: Intravesical instillation of TCDCA every other day for 1 week (1 h per session). TLR3 inhibitor group: Same intravesical TCDCA instillation as above, followed by intraperitoneal injection of a TLR3 inhibitor (CU-CPT 4a, MCE, Cat. HY-108473) at 1 mg/kg[47], twice per week for 2 weeks. PPS treatment group: Same intravesical TCDCA instillation as above, followed by oral gavage of PPS at 31.25 mg/kg[5], 5 times per week for 2 weeks. Following treatment, behavioral changes and pain scores were assessed, after which animals were euthanized by carbon dioxide (CO_2) inhalation followed by cervical dislocation for histopathological evaluation of bladder tissues across groups.

Statistical analysis

Statistical analyses and graph generation were conducted using R (version 3.6.1) and GraphPad Prism software (version 8.0). Continuous variables were reported as median (IQR) or means ± standard deviation (SD), and group comparisons were performed using the Mann–Whitney *U* test or Kruskal–Wallis test. A *p*-value less than 0.05 was considered statistically significant.

Reporting summary

Further information on research design is available in the Nature Portfolio Reporting Summary linked to this article.

Data availability

Raw human fecal 16S rRNA sequencing data have been deposited in the NCBI BioProject database under accession PRJNA1380896 (https://www.ncbi.nlm.nih.gov/bioproject/?term=1380896). Human fecal metagenomic sequencing data are available in the NCBI under BioProject accession PRJNA1367514. Raw non-targeted metabolomics data have been deposited in the MetaboLights database, including blood metabolomics (MTBLS13512; https://www.ebi.ac.uk/metabolights/MTBLS13512) and urine metabolomics (MTBLS13513; https://www.ebi.ac.uk/metabolights/MTBLS13513). Bulk RNA-seq datasets were obtained from the Gene Expression Omnibus (GEO) database under accession numbers GSE238208 (HIC samples; https://www.ncbi.nlm.nih.gov/geo/query/acc.cgi?acc=GSE238208) and GSE11783 (control samples; https://www.ncbi.nlm.nih.gov/geo/query/acc.cgi?acc=GSE11783). Single-cell RNA sequencing data have been deposited in GEO under accession GSE310557. Mouse fecal metagenomic sequencing data are available in the NCBI BioProject database under accession PRJNA1381332 (https://www.ncbi.nlm.nih.gov/bioproject/?term=1381332). Targeted bile acid metabolomics data for blood and urine are included in Supplementary Tables 5 and 6, respectively. All data supporting the findings described in this manuscript are available in the article and in the Supplementary Information and from the corresponding author upon request. Source data are provided with this paper.

Code availability

No custom code was used in this study.

References

1. Mohammad, A., Laboulaye, M. A., Shenhar, C. & Dobberfuhl, A. D. Mechanisms of oxidative stress in interstitial cystitis/bladder pain syndrome. *Nat. Rev. Urol.* **21**, 433–449 (2024).
2. Clemens, J. Q., Erickson, D. R., Varela, N. P. & Lai, H. H. Diagnosis and treatment of interstitial cystitis/bladder pain syndrome. *J. Urol.* **208**, 34–42 (2022).
3. Dellis, A. E. & Papatsoris, A. G. Bridging pharmacotherapy and minimally invasive surgery in interstitial cystitis/bladder pain syndrome treatment. *Expert Opin. Pharmacother.* **19**, 1369–1373 (2018).
4. Peng, L. et al. Integrating single-cell RNA sequencing with spatial transcriptomics reveals immune landscape for interstitial cystitis. *Signal Transduct. Target Ther.* **7**, 161 (2022).
5. Peng, L. et al. UPK3A(+) umbrella cell damage mediated by TLR3-NR2F6 triggers programmed destruction of urothelium in Hunner-type interstitial cystitis/painful bladder syndrome. *J. Pathol.* **263**, 203–216 (2024).
6. Braundmeier-Fleming, A. et al. Stool-based biomarkers of interstitial cystitis/bladder pain syndrome. *Sci. Rep.* **6**, 26083 (2016).
7. Xu, H. et al. Combined signature of the urinary microbiome and metabolome in patients with interstitial cystitis. *Front. Cell Infect. Microbiol.* **11**, 711746 (2021).

8. Zheng, Z. et al. Integrated microbiome and metabolome analysis reveals novel urinary microenvironmental signatures in interstitial cystitis/bladder pain syndrome patients. *J. Transl. Med.* **21**, 266 (2023).
9. Torimoto, K. et al. Serum anandamide and lipids associated with linoleic acid can distinguish interstitial cystitis/bladder pain syndrome from overactive bladder: an exploratory study. *Low. Urinary Trac. Symptoms* **15**, 238–246 (2023).
10. Tian, J. H. et al. Clustering of urinary biomarkers to identify interstitial cystitis subtypes and different clinical characteristics and treatment outcomes. *Biomedicines* **13**, 369 (2025).
11. Chen, Y. C. & Kuo, H. C. Integrating biomarker clustering for improved diagnosis of interstitial cystitis/bladder pain syndrome: a review. *Int. Urol. Nephrol.* **57**, 2725–2734 (2025).
12. Fu, C. et al. The microbiota in patients with interstitial cystitis/bladder pain syndrome: a systematic review. *BJU Int.* **134**, 869–880 (2024).
13. Magalhaes, T. F., Baracat, E. C., Doumouchtsis, S. K. & Haddad, J. M. Biomarkers in the diagnosis and symptom assessment of patients with bladder pain syndrome: a systematic review. *Int. Urogynecol. J.* **30**, 1785–1794 (2019).
14. Lai, H. H., Pickersgill, N. A. & Vetter, J. M. Hunner lesion phenotype in interstitial cystitis/bladder pain syndrome: a systematic review and meta-analysis. *J. Urol.* **204**, 518–523 (2020).
15. Caldwell, A. et al. TGR5 agonists induce peripheral and central hypersensitivity to bladder distension. *Sci. Rep.* **12**, 9920 (2022).
16. Jhang, J. F. & Kuo, H. C. Bladder dysfunction in 2016: new insights into interstitial cystitis and chronic pelvic pain syndromes. *Nat. Rev. Urol.* **14**, 69–70 (2017).
17. Dalghi, M. G., Montalbetti, N., Carattino, M. D. & Apodaca, G. The Urothelium: life in a liquid environment. *Physiol. Rev.* **100**, 1621–1705 (2020).
18. Lu, M., Zhu, K., Schulam, P. G. & Chai, T. C. A non-enzymatic method for dissection of mouse bladder urothelial tissue. *Nat. Protoc.* **14**, 1280–1292 (2019).
19. Zhao, Q. et al. Parabacteroides distasonis ameliorates hepatic fibrosis potentially via modulating intestinal bile acid metabolism and hepatocyte pyroptosis in male mice. *Nat. Commun.* **14**, 1829 (2023).
20. Park, S., Aintablian, A., Coupe, B. & Bouret, S. G. The endoplasmic reticulum stress-autophagy pathway controls hypothalamic development and energy balance regulation in leptin-deficient neonates. *Nat. Commun.* **11**, 1914 (2020).
21. Farnsworth, T. A. Enterococcus avium splenic abscess: a rare bird. *Lancet Infect. Dis.* **2**, 765 (2002).
22. Verhaegen, J., Pattyn, P., Hinnekens, P. & Colaert, J. Isolation of Enterococcus avium from bile and blood in a patient with acute cholecystitis. *J. Infect.* **35**, 77–78 (1997).
23. Patel, R., Keating, M. R., Cockerill, F. R. 3rd & Steckelberg, J. M. Bacteremia due to Enterococcus avium. *Clin. Infect. Dis.* **17**, 1006–1011 (1993).
24. Anderson, V. R. & Perry, C. M. Pentosan polysulfate: a review of its use in the relief of bladder pain or discomfort in interstitial cystitis. *Drugs* **66**, 821–835 (2006).
25. Jhang, J. F., Yu, W. R., Jiang, Y. H. & Kuo, H. C. Pathophysiology and potential multimodal therapeutic strategies for IC/BPS. *Nat. Rev. Urol.* **22**, 672–686 (2025).
26. Bullock, A. D., Becich, M. J., Klutke, C. G. & Ratliff, T. L. Experimental autoimmune cystitis: a potential murine model for ulcerative interstitial cystitis. *J. Urol.* **148**, 1951–1956 (1992).
27. Lin, Y. H. et al. Lower urinary tract phenotype of experimental autoimmune cystitis in mouse: a potential animal model for interstitial cystitis. *BJU Int.* **102**, 1724–1730 (2008).
28. Jin, X. W., Liu, B. K., Zhang, X., Zhao, Z. H. & Shao, Y. Establishment of a novel autoimmune experimental model of bladder pain syndrome/interstitial cystitis in C57BL/6 mice. *Inflammation* **40**, 861–870 (2017).
29. Peng, L. et al. Identification of key genes in human urothelial cells corresponding to interstitial cystitis/bladder pain syndrome in a lipopolysaccharide-induced cystitis model. *Neurourol. Urodyn.* **40**, 1720–1729 (2021).
30. Su, F. et al. Multimodal single-cell analyses outline the immune microenvironment and therapeutic effectors of interstitial cystitis/bladder pain syndrome. *Adv. Sci.* **9**, e2106063 (2022).
31. Lamale, L. M., Lutgendorf, S. K., Zimmerman, M. B. & Kreder, K. J. Interleukin-6, histamine, and methylhistamine as diagnostic markers for interstitial cystitis. *Urology* **68**, 702–706 (2006).
32. Peng, L. et al. Metabolic syndrome in women with and without interstitial cystitis/bladder pain syndrome. *Int. Urogynecol. J.* **32**, 1299–1306 (2020).
33. Kim, J. et al. Diagnostic utility of serum and urinary metabolite analysis in patients with interstitial cystitis/painful bladder syndrome. *Urology* **157**, 85–92 (2021).
34. Hanno, P. M., Landis, J. R., Matthews-Cook, Y., Kusek, J. & Nyberg, L. Jr. The diagnosis of interstitial cystitis revisited: lessons learned from the National Institutes of Health Interstitial Cystitis Database study. *J. Urol.* **161**, 553–557 (1999).
35. Kuret, T., Sterle, I., Romih, R. & Veranič, P. Matched serum- and urine-derived biomarkers of interstitial cystitis/bladder pain syndrome. *PLoS One* **19**, e0309815 (2024).
36. Joyce, C., Halverson, T., Gonzalez, C., Brubaker, L. & Wolfe, A. J. The urobiomes of adult women with various lower urinary tract symptoms status differ: a re-analysis. *Front. Cell Infect. Microbiol.* **12**, 860408 (2022).
37. Roje, B. et al. Gut microbiota carcinogen metabolism causes distal tissue tumours. *Nature* **632**, 1137–1144 (2024).
38. Jia, D. et al. Microbial metabolite enhances immunotherapy efficacy by modulating T cell stemness in pan-cancer. *Cell* **187**, 1651–1665.e1621 (2024).
39. Zhang, X. J. et al. Pharmacological inhibition of arachidonate 12-lipoxygenase ameliorates myocardial ischemia-reperfusion injury in multiple species. *Cell Metab.* **33**, 2059–2075.e2010 (2021).
40. Pan, Q. et al. A homozygous R148W mutation in Semaphorin 7A causes progressive familial intrahepatic cholestasis. *EMBO Mol. Med.* **13**, e14563 (2021).
41. Won, T. H. et al. Host metabolism balances microbial regulation of bile acid signalling. *Nature* **638**, 216–224 (2025).
42. Argaw-Denboba, A. et al. Paternal microbiome perturbations impact offspring fitness. *Nature* **629**, 652–659 (2024).
43. Lloyd-Price, J. et al. Multi-omics of the gut microbial ecosystem in inflammatory bowel diseases. *Nature* **569**, 655–662 (2019).
44. Zarrinpar, A. et al. Antibiotic-induced microbiome depletion alters metabolic homeostasis by affecting gut signaling and colonic metabolism. *Nat. Commun.* **9**, 2872 (2018).
45. Saavedra, P. H. V. et al. Broad-spectrum antibiotics disrupt homeostatic efferocytosis. *Nat. Metab.* **6**, 1682–1694 (2024).
46. AlJindan, R. et al. Phenomics and genomic features of Enterococcus avium IRMC1622a isolated from a clinical sample of hospitalized patient. *J. Infect. Public Health* **17**, 102463 (2024).
47. Nakai, K. et al. Wnt activation disturbs cell competition and causes diffuse invasion of transformed cells through NF-κB-MMP21 pathway. *Nat. Commun.* **14**, 7048 (2023).

Acknowledgements

We thank Ms Ziyuan Xia for her support in sample testing. This study was funded by 1.3.5 project for disciplines of excellence, West China Hospital, Sichuan University (ZYYC25003), the National Natural Science Fund of China (82422015, 82270720, 82400904, and 82500827), China Postdoctoral Science Foundation (2024M752250 and 2025T180613),

and Postdoctoral Science Foundation of West China Hospital (2024HXBH108).

Author contributions

H.S., T.J., Q.S. and D.Y.L. directed the research. L.P., B.Y.L., C.Z., X.P.D., L.D.L., Y.Z.C., and J.W.C. designed the project and experiments. L.P., Y.Z.C., L.D.L., W.W., Y.C.M., S.H.S., and H.R.L. performed the experiments and analyzed the data. X.S.G. and X.Z. assisted in the experiments. X.F.X. and Y.Z.C. performed cell isolation, identification, and culture, as well as the fecal microbiota transplantation experiments. B.Y.L., C.Z., and H.R.L. collected the samples from patients. L.P. wrote the manuscript. L.D.L. and D.Y.L edited the manuscript. All authors reviewed and commented on the manuscript.

Competing interests

The authors declare no competing interests.

Additional information

Supplementary information The online version contains supplementary material available at https://doi.org/10.1038/s41467-025-68060-1.

Correspondence and requests for materials should be addressed to Qun Sun, Tao Jin or De-yi Luo.

Peer review information *Nature Communications* thanks Thomas Hannan, Yousheng Yao, Fei Xiao, and the other, anonymous, reviewer(s) for their contribution to the peer review of this work. A peer review file is available.